Sustainability in Environment
ISSN 2470-637X (Print) ISSN 2470-6388 (Online)
Vol. 10, No. 2, 2025
www.scholink.org/ojs/index.php/se

*Original Paper*

# Application of Fast Fourier Transform-based Method for the Thermal System of Buried Pipe Heat Exchanger

Wei Yang[1,*], Ruiling Yu[1], Chenchen Bao[1], Manfeng Li[1] & Linlin Zhang[1]

[1] School of Environmental & Municipal Engineering, North China University of Water Resources and Electric Power, Zhengzhou 450046, P. R. China

* Wei Yang, School of Environmental & Municipal Engineering, North China University of Water Resources and Electric Power, Zhengzhou 450046, P. R. China

Received: February 23, 2025 Accepted: April 02, 2025 Online Published: April 21, 2025

doi:10.22158/se.v10n2p41 URL: http://dx.doi.org/10.22158/se.v10n2p41

***Abstract***

*The Fourier transform method for discrete sequences is introduced in this study and applied to decompose the heat flux per unit borehole depth in buried pipe heat exchangers (BPHE) into a summation of Fourier series. The linear relationship between the heat flux per unit borehole depth in BPHE and the cooling and heating load of Ground-Coupled Heat Pumps (GCHP) is delineated. It is demonstrated that, similar to the cooling and heating load of GCHP, the heat flux per unit borehole depth in BPHE exhibits a general trend with periodic variability on an annual scale (8760 hours). The Fourier transform of discrete sequences enables the representation of the heat flux per unit borehole depth in BPHE as a summation of Fourier series, comprising a Step Heat Flux (direct current components) and heat flux in trigonometric forms. Further investigation reveals that the heat flux in trigonometric form does not influence the long-term average temperature of the surrounding soil and rock, whereas the Step Heat Flux significantly affects it. Therefore, the long-term performance of BPHE is predominantly governed by the Step Heat Flux.*

***Keywords***

*Ground-Coupled Heat Pumps, The finite line source model, Fast Fourier transform, Thermal response modeling.*

## 1. Introduction

Geothermal energy plays a vital role in achieving carbon neutrality. However, compared to other renewable energy sources, its utilization remains relatively low, emphasizing the urgent need for more efficient exploitation of geothermal resources (Liang, Tu, Zeng, Zhang, Cheng, & Luo, 2023). Ground

Source Heat Pump (GSHP) systems, which harness geothermal energy for heating and cooling, experienced a steady rise in adoption rates between 2010 and 2015 (Smith, & Taylor, 2023). Due to their high energy efficiency, low electricity consumption, and potential for reducing greenhouse gas emissions, these systems have attracted significant attention in recent years (Kitsopoulou, Zacharis, et al, 2023).

GSHP systems utilize soil as a thermal source or sink (Narsilio, 2018; Kurevija, Macenić, & Galović, 2025), benefiting from the stable temperature characteristics of subsurface layers at certain depths (Wu, Hou, Su, & Ma, 2024). This stability is influenced by the decreasing variability in ground temperature with increasing depth, which is determined by the composition of the soil and rock. Consequently, these relatively constant temperatures offer favorable conditions for the deployment of GSHP systems. Two primary configurations of GSHP systems exist: horizontal and vertical layouts (Cheruy, Dufresne, et al, 2017). Compared to horizontal systems, vertical configurations require less surface area, provide a more stable thermal source, and exhibit higher operational efficiency. Vertical systems typically employ BPHEs integrated with heat pumps.

A common configuration of BPHEs is a vertical closed-loop system, which features a U-shaped tube made of high-density polyethylene installed within a vertical borehole (Zhou, Narsilio et al, 2024). The performance of BPHEs is critical to the success of GSHP systems, as it directly affects the amount of heat energy extracted or rejected. This performance must be sufficient to meet the thermal energy demands throughout the system's lifecycle. Over the last decade, the deployment of BPHEs has significantly increased, particularly in urban areas of Central and Northern Europe, the United States, and China (Miglani, Orehounig, & Carmeliet, 2018). This trend highlights the increasing necessity of accurately predicting BPHE performance to ensure efficient and reliable system operation.

## 2. Data Acquisition

### *2.1 Generation Load*

In this study, an office building located in Changsha was selected for analysis. A detailed model was developed using Design Builder software. Meteorological data from a typical year in Changsha were utilized to compute the building's hourly cooling and heating loads over an entire year (8760 hours). These results are depicted in Figure 1. Positive values in the graph represent cooling loads, which correspond to the building's heat emission, while negative values denote heating loads, indicating heat absorption by the building.

Simulation outcomes show that the office building's total annual cooling load amounts to $1.161\times10^{5}$ kW, while the total annual heating load equals $-7.432\times10^{4}$ kW. The peak hourly cooling load is observed to be $q_{lc,max}=90.96$ kW, and the maximum hourly heating load is recorded at $q_{lh,max}=-59.40$ kW.

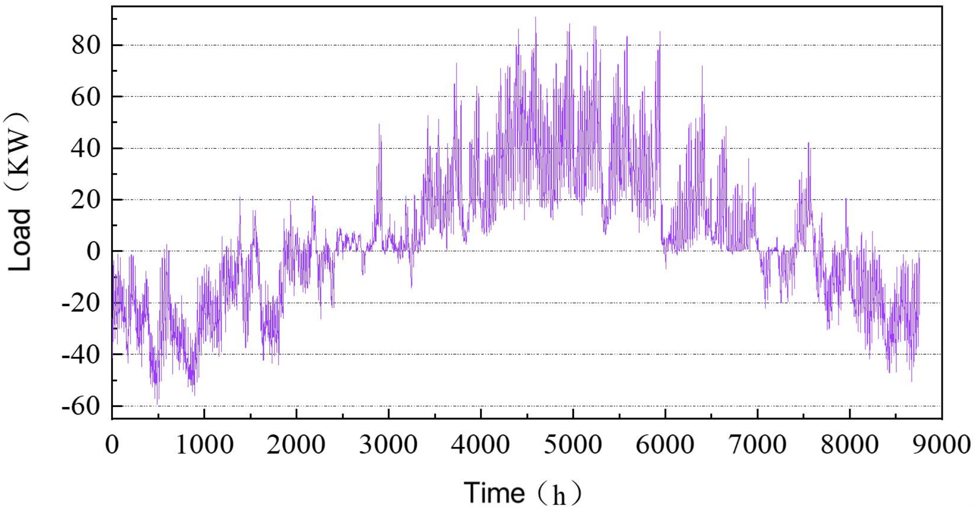


**Figure 1. Hourly Variation of Cooling and Heating Loads for an Office Building in Changsha**

*2.2 Determination of Total Drilling Depth for BPHE*

To determine the heat flux per unit depth exerted on the BPHE, the total required borehole depth must first be calculated. Reference (Diao & Fang, 2016) provides an estimated index for heat transfer per unit borehole depth in BPHE for North China, as outlined in Table 1. Using these indices and assuming the maximum heat transfer capacity H of the BPHE is 60 W/m per meter of borehole depth, the total drilling length needed to meet the maximum cooling and heating loads of the system can be computed using the formula below (Wu, Li, & Zhang, 2025; Qian, Wu, et al, 2021).

$$l = \frac{\max\left(Q_{lc,\max}, Q_{lh,\max}\right)}{q_l} \tag{1}$$

Upon substituting the relevant parameters into the formula, the calculated result yields a total drilling length of l = 1516 m.

**Table 1. Preliminary Estimate Indices for BPHE Design Solutions**

| Buried pipe form | | Unit borehole depth heat exchange (W/m) | | | The ratio of building area to buried pipe area | | |
|---|---|---|---|---|---|---|---|
| | | Soil layer | Geotechnical layer | Rock layer | Soil layer | Geotechnical layer | Rock layer |
| Vertical buried pipe | Single U-shaped buried pipe | 30~40 | 40~50 | 50~60 | 3:1 | 4:1 | 5:1 |
| | Dual U-shaped buried pipe | 36~48 | 48~60 | 60~72 | 4:1 | 5:1 | 6:1 |

*2.3 Determination of heat flux per Unit Borehole Depth exerted on BPHE*

In conventional Ground-Coupled Heat Pump (GCHP) systems, during cooling conditions, the heat pump units exchange heat through the condenser in conjunction with the Buried Pipe Heat Exchanger (BPHE), effectively dissipating thermal energy into the surrounding rock and soil. Conversely, during heating operations, the heat pump units perform heat exchange through the evaporator in conjunction with the BPHE, absorbing thermal energy from the rock and soil. In direct expansion ground-source heat pump systems, the BPHE serves as a condenser during cooling conditions, directly transferring heat into the rock and soil, while during heating operations, it functions as an evaporator, extracting thermal energy from the rock and soil (Cao, Zhou, et al , 2023).

The heat release and absorption associated with the BPHE include: (1) the heat release and absorption driven by the cooling and heating load of the air conditioning system, (2) the heat discharged by the water pump into the circulating water, (3) the thermal changes in the circulating water during its flow. It is noted that the heat discharged into the circulating water by the water pump, as well as the thermal changes encountered by the circulating water during its conveyance, represent minor quantities compared to the thermal exchanges induced by the air conditioning system's cooling and heating load. Consequently, these minor quantities are omitted from consideration. At this point, the thermal flux exerted on the BPHE demonstrates a linear relationship with the cooling and heating load of the GCHP system. During cooling operations, the heat flux exerted on the BPHE is expressed as:

$$Q_{lc} = Q_c\left(1 + \frac{1}{COP}\right) \tag{2}$$

Where: $Q_{lc}$ represents the heat flux exerted on the BPHE during cooling conditions (W); $Q_c$ corresponds to the cooling load of the GCHP system (W); COP represents the coefficient of performance of the GCHP unit.

Assuming the total borehole length of the BPHE is *l* meters, the heat flux $q_l$ per unit borehole depth exerted on the BPHE is given by:

$$q_l = \frac{Q_{lc}}{l} \tag{3}$$

Thus:

$$q_l = Q_c\left(1 + \frac{1}{COP}\right)/\,l \tag{4}$$

Similarly, during heating operations, the heat flux $Q_{lh}$ exerted on the BPHE is defined as:

$$Q_{lh} = Q_h\left(1 - \frac{1}{EER}\right) \tag{5}$$

Where, $Q_h$ denotes the heating load of the GCHP unit during heating operations (W), EER represents the heating coefficient of the GCHP unit.

Therefore, during heating operations, the heat flux $q_l$ per unit borehole depth exerted on the BPHE is established as:

$$q_l = Q_h\left(1-\frac{1}{EER}\right)/l \tag{6}$$

Given that the system's cooling and heating loads $Q_c$ and $Q_h$, as defined by Design Builder (refer to Figure 1), and the required total borehole depth for the BPHE (l = 1516 m), are predetermined, it is assumed that the values for COP and EER remain constant at 4.0 throughout the operational life of the heat pump unit. The corresponding heat flux per unit borehole depth can be calculated. The results of these calculations are shown in Figure 2.

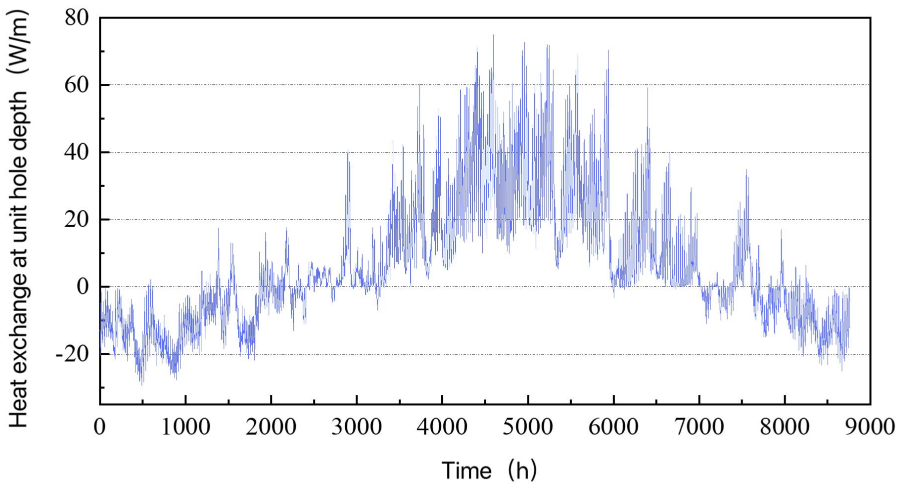


**Figure 2. Hourly Heat Flux per unit Borehole Depth of the BPHE in an Office Building in Changsha**

## 3. Methodology

*3.1 Fourier Series Representation of Unit Borehole heat flux exerted on Buried Pipe Heat Exchanger*

The heat flux exerted on the BPHE is influenced by the cooling and heating load generated by the Ground-Coupled Heat Pump (GCHP) system. These loads are closely linked to local meteorological conditions, which vary on hourly, daily, monthly, and seasonal bases. Over short timeframes, such as daily cycles, cooling and heating loads exhibit 24-hour cyclical variations. Over longer periods, such as annually, these loads follow a cycle lasting 8760 hours.

While the cooling and heating load primarily display cyclical fluctuations, they also exhibit elements of randomness and irregularity. Nevertheless, a complex, non-simple harmonic motion periodic function can be expressed as a summation of sine (or cosine) terms. Consequently, as explained in the preceding sections, discrete sequences can be transformed into summable Fourier series. A linear relationship exists between the heat flux $q_l$ per unit borehole depth exerted on the BPHE and the cooling and heating load of the GCHP system. Therefore, the heat flux per unit borehole depth on the BPHE can also be approximated as a complex periodic function of non-simple harmonic motion (Wang, Zhang, &

Zhao, 2024). When transformed into a Fourier series, the temperature response of the BPHE under irregular heat flow conditions can be simplified into the response to periodic sinusoidal (or cosine) heat fluxes, thereby reducing the complexity of the analysis (Zhang, & Huang, 2023).

Using the foundational principles and methodologies for applying the Fast Fourier Transform (FFT) to discrete sequences (Orian, Yahav, et al, 2023; Moulinec, Suquet, 1994; Moulinec, 1995), the hourly heat flux per unit borehole depth impacting the BPHE undergoes a Fourier transform, implemented via MATLAB programming (Zhang, & Wang, 2023; Mariam, 2023).

By leveraging MATLAB programming, the heat flux with an annual period (T = 8760 hours, N = 8760 data points) is decomposed into a step heat flux (direct current components) $a_0$ and the summation of (N/2-1) heat fluxes represented as trigonometric functions, as shown in the formula below:

$$q_l(\tau) = a_0 + \sum_{i=2}^{N/2} A_i \sin\left(\frac{2\pi}{T_i}\tau + \phi_i\right) \tag{7}$$

Where $A_i$ —The amplitude of the heat flux pertaining to the ith order sinusoidal wave, W/m;

$a_0$ —The step heat flux, representing the system's direct current component and the mean annual heat flux exerted on the BPHE, W/m;

$T_i$ —The period of the heat flux corresponding to the ith order sinusoidal wave, h;

$\phi_i$ —The phase angle of the ith order sinusoidal heat flux, rad.

*3.2 The Finite Line Source Model*

In heat transfer analysis of the Buried Pipe Heat Exchanger (BPHE) in Ground-Coupled Heat Pump (GCHP) systems, the surrounding rock and soil are typically modeled as a semi-infinite medium. Boreholes containing heat exchange pipes are approximated as line heat sources within this medium. Traditional models, such as the one-dimensional Kelvin line heat source model and the one-dimensional cylindrical borehole heat transfer model, fail to achieve a stable temperature field when the time approaches infinity if the annual heat absorption and discharge of the BPHE are unbalanced. As a result, these models are unsuitable for analyzing long-term thermal behaviors. The finite line source model, however, incorporates the ground as a boundary condition, making it ideal for long-term analysis.

The finite line source model (FLS) is used to predict ground temperature variations in geothermal bore fields comprising vertical geothermal boreholes. Its primary applications include evaluating thermal response factors (g-functions) (Rekeraho, Cotfas, et al, 2025), which are later utilized to design (Ahmadfard, & Bernier, 2019), simulate (Mitchell & Spitler, 2019), and control (Choi, Choi, & Lee, 2023) geothermal systems. Furthermore, the model can be superimposed in both time and space to construct detailed representations of geothermal systems (Lazzarotto, 2014; Lamarche, 2017). Below, the mathematical framework of the finite line source model is introduced.

3.2.1 Mathematical Model

Figure 3 depicts a semi-infinite medium with an initial uniform temperature, $t_0$. The boundary of this medium, specifically the surface at z=0, is assumed to maintain a constant temperature $t_0$. A finite-length uniform line heat source with intensity $q_l$ (W/m), perpendicular to the boundary surface, initiates heat rejection or absorption. Due to symmetry, the resulting temperature distribution in cylindrical coordinates is two-dimensional. By setting the surface temperature of the medium $t_0$ as the zero point of excess temperature, and applying the virtual source method, that is, set $\theta = t - t_0$. By using the virtual heat-source method, the virtual heat-source with an intensity of -$q_l$ and of comparable length, H, is placed opposite the line heat source boundary, thereby automatically adhering to the constant temperature boundary condition (Kurevija, Macenić, & Galović, 2025).

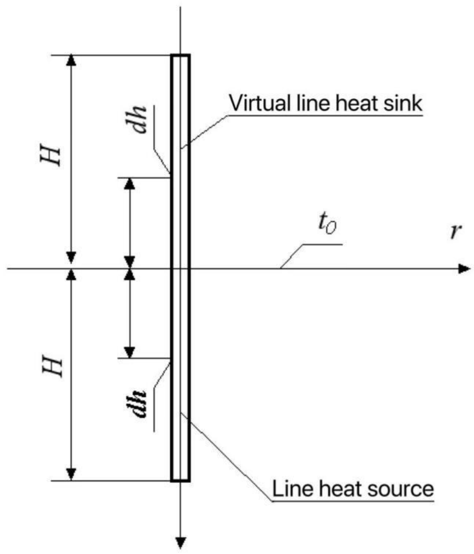


**Figure 3. Line Heat Source and Line Heat Sink and Their Geometrical Relationship**

Due to the linear nature of the problem, the excess temperature at point B in cylindrical coordinates at time A is derived from the cumulative contributions of infinitesimal segments along the line heat source and the virtual heat source. The resulting expression is (Diao & Fang, 2006):

$$\theta = \frac{q_l}{4\pi\lambda_s}\int_0^H \left\{ \frac{erfc\left[\frac{\sqrt{r^2+(z-h)^2}}{2\sqrt{a\tau}}\right]}{\sqrt{r^2+(z-h)^2}} - \frac{erfc\left[\frac{\sqrt{r^2+(z+h)^2}}{2\sqrt{a\tau}}\right]}{\sqrt{r^2+(z+h)^2}} \right\} dh \tag{8}$$

Here, 'X' represents the thermal conductivity and 'a' denotes the thermal diffusivity of the soil surrounding the BPHE. The complementary error function, 'erfc(z)', is defined as:

$$erfc(z) = 1 - \frac{2}{\sqrt{\pi}}\int_0^z \exp(-u^2)du \tag{9}$$

Nondimensionalizing Formula (8) by setting $Z = \frac{z}{H}$, $H' = \frac{h}{H}$, $R = \frac{r}{H}$ $Fo = \frac{a\tau}{H^2}$,

$\Theta = \dfrac{4\lambda\pi(t-t_0)}{q_l}$ results in:

$$\Theta = \int_0^1 \left[ \frac{erfc\left[\dfrac{\sqrt{R^2+(Z-H')^2}}{2\sqrt{Fo}}\right]}{\sqrt{R^2+(z-H')^2}} - \frac{erfc\left[\dfrac{\sqrt{R^2+(Z+H')^2}}{2\sqrt{Fo}}\right]}{\sqrt{R^2+(z+H')^2}} \right] dH' \tag{10}$$

The dimensionless temperature $\Theta$ is shown to depend on the non-dimensional variables Z, R, And the Fourier number $Fo$ ,that is $\Theta = f\left(z, R, Fo\right)$.

When Z = 0.5 and R be defined as the relative radius $R_b = r_b / H$ the borehole wall, then the nondimensional temperature $\Theta_b$ the median point of the borehole wall emerges as a function of both $R_b$ d Fo. When $Fo \to \infty$ the unsteady temperature field transitions towards a state of stable temperature field, for which the analytical expressions is delineated in reference (Diao & Fang, 2006):

$$\Theta = \ln\left[\frac{\sqrt{R^2+(1-Z)^2}+1-Z}{\sqrt{R^2+(1+Z)^2}+1+Z} \cdot \frac{2Z^2+2Z\sqrt{R^2+Z^2}+R^2}{R^2}\right] \tag{11}$$

This formula indicates that, in a steady-state temperature field, the dimensionless temperature $\Theta$ depends solely on the non-dimensional parameters Z and R.

An approximate relationship between the integral average temperature response of the borehole wall and the relative radius is derived in reference through linear regression:

$$\overline{\theta}_b \approx \frac{q_l}{2\pi\lambda_s} \ln\frac{H}{2.7r_b} \tag{12}$$

A comparative analysis with the precise value of the integrated average temperature reveals that for $0.0005 < r_b/H < 0.005$, the relative error inherent in Formula 12 is discovered to be less than 0.09%.

*3.3. Method and Route*

The heat flux per unit borehole depth on the BPHE exhibits a linear relationship with the cooling and heating load of the GCHP system. Consequently, similar to the cooling and heating load of the GCHP system, the heat flux predominantly follows an annual cyclic variation of 8760 hours. By applying the Fourier transform approach to discrete series, the heat flux per unit borehole depth on the BPHE can be expressed as a summation of Fourier series. It can be decomposed into a step heat flux (direct current components) and a series of heat flux in trigonometric forms, thereby significantly simplifying the analysis. For evaluating the temperature response within the soil surrounding the BPHE, it suffices to analyze the response under the influence of a step heat flux and sinusoidal (or cosine) functions of heat flux.

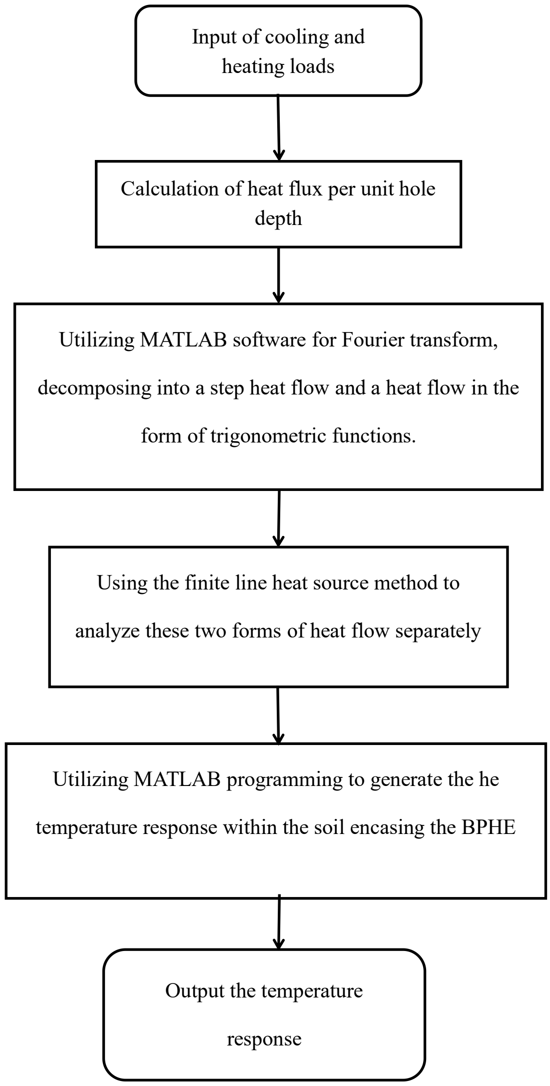


**Figure 4. The Program Design Flowchart for Solving Temperature Response Using the Fast Fourier Transform Method**

## 4. Results and Analysis

*4.1 Temperature Response and Its Steady-State Solution Under Step Heat Flux Action*

4.1.1 Temperature Response Under Step Heat Flux Action

A continuous, constant heat flow starting from the initial moment is referred to as a step heat flow. Analyzing the temperature response at the borehole wall of the BPHE under step heat flow conditions forms the basis for understanding the exchanger's behavior under various heat flow scenarios. Initially, a detailed analysis of this phenomenon is presented. Figure 5 illustrates the schematic representation of a step heat flow with magnitude A, commencing from time zero.

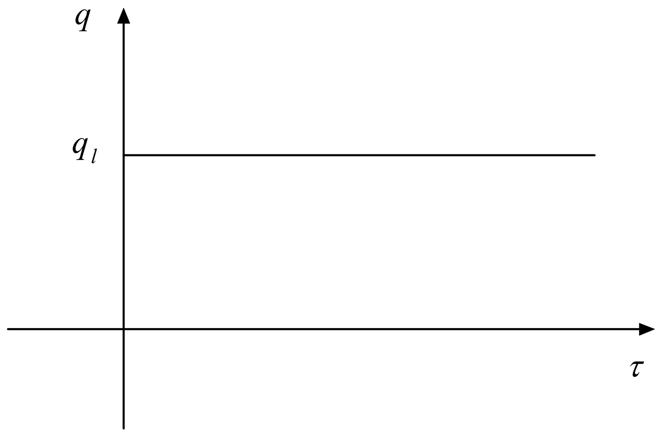


**Figure 5. Schematic of the Step Heat Flow of Magnitude A Commencing from the Zero Moment**

**Table 2. Basic Parameters of the BPHE and Surrounding Rock**

| Depth from the ground $z$(m) | pipe buried depth $H$(m) | The vertical distance from the line heat source $r$ (m) | thermal conductivity $\lambda_s$ (W/m·K) | Diffusion rate of rock $a$ ($m^2/s$) | Dimensionless depth $Z$ ($z/H$) | Dimensionless vertical distance from line heat source $R$ ( $r/H$) |
|---|---|---|---|---|---|---|
| 30 | 60 | 0.065 | 2.1 | $1.2\times10^{-6}$ | 0.5 | 0.0021667 |

Based on parameters in Table 2, the application of step heat flow causes the temperature response at the borehole wall to initially rise rapidly and then stabilize. The dimensionless excess temperature remains unaffected by the heat flux magnitude, with its variation pattern shown in Figure 6.

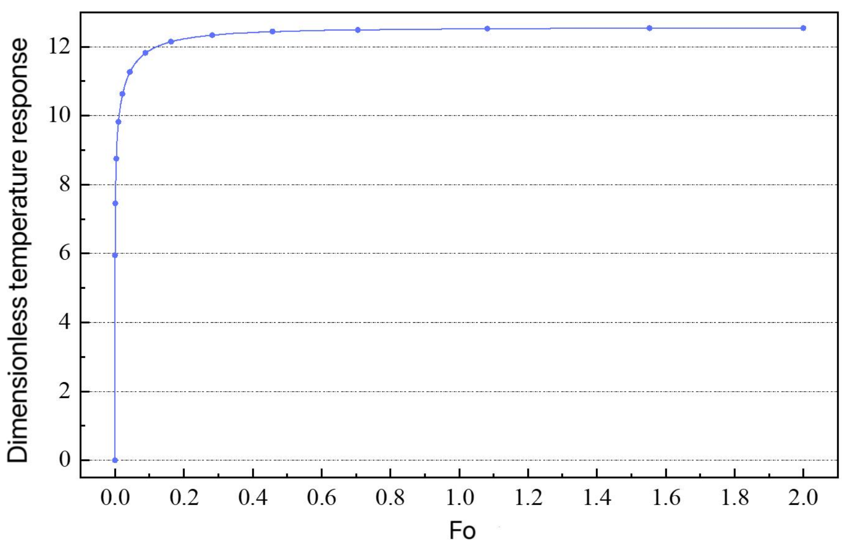


**Figure 6. Dimensionless Temperature Response at the Borehole Wall under Step Heat Flow**

The actual temperature response of the BPHE is influenced by the heat flux magnitude. A larger heat flux results in a greater temperature response, while a smaller heat flux leads to a reduced response, as shown in Figure 7.

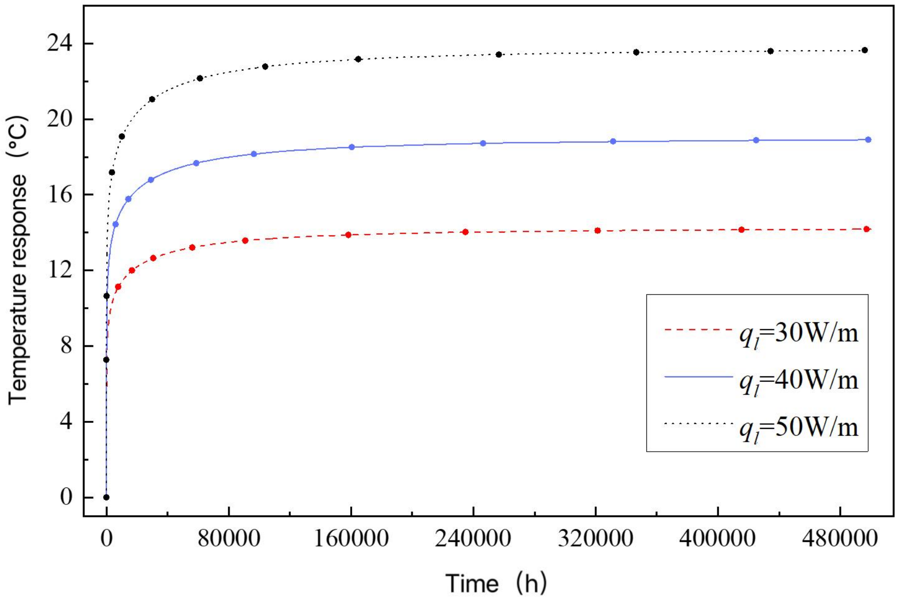


**Figure 7. Temperature Response at the Borehole wall under Different Step Heat Flows**

4.1.2 Steady-State Solution and Its Significance of Temperature Response Induced by Step Heat Flux

Figure 7 reveals that in the presence of a step heat flow, the temperature response converges to a constant value for sufficiently large time intervals. This constant value represents the steady-state solution of temperature response attributed to the step heat flow. The computation of the steady-state solution for the temperature response resulting from step heat flows can be accomplished through MATLAB programming, employing the method of limit calculation with respect to time. The computational outcomes from MATLAB are summarized in Table 3, which enumerates the values of steady-state solutions for temperature responses caused by varying magnitudes of step heat flows. Table 3 illustrates a linear correlation between the steady-state solutions of temperature responses and the intensity of step heat flows.

**Table 3. Steady-State Solutions of Temperature Responses under Step Heat Flows of Different Magnitudes**

| Step Heat Flows (W/m) | 10 | 20 | 30 | 40 | 50 |
|---|---|---|---|---|---|
| the steady-state solutions of temperature responses (°C) | 4.7853 | 9.5706 | 14.3559 | 19.1412 | 23.9265 |

The lesser the radial vertical distance from the finite line source, the greater the steady-state solutions of temperature responses of a step heat flow. As the radial distance expands, the value initially declines swiftly. Following this, the rate of change decelerates gradually, as demonstrated in Figure 8, with the step heat flow $q_l$ =50 W/m and other parameters consistent with those featured in Table 2.

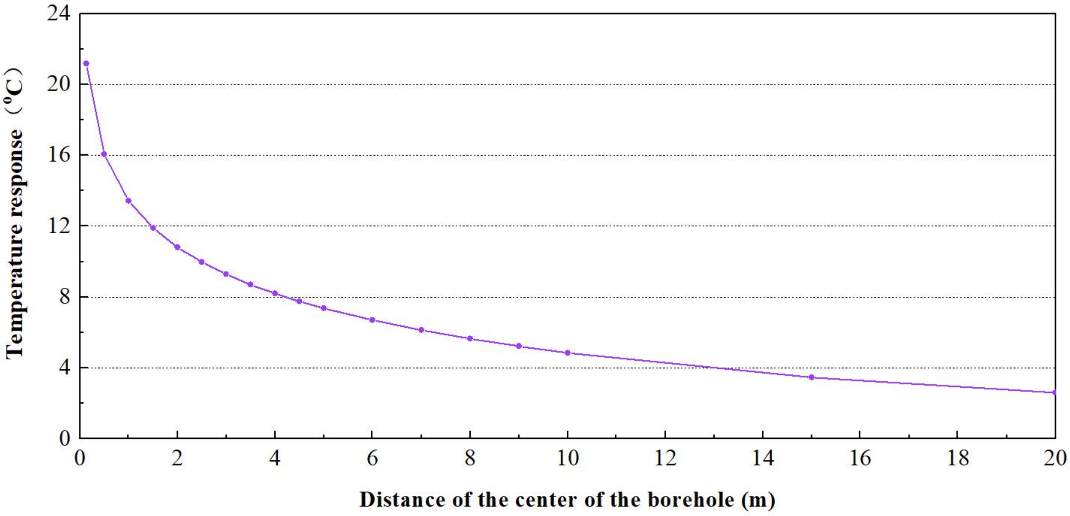


**Figure 8. Radial Steady-state Temperature Response Variation at Different Distances from the Center of the Borehole**

According to the FLS, the temperature response gradually from an unsteady to a steady state temperature field over time. The steady state temperature field is critically important for both the design of BPHE and the evaluation of their long-term performance. It is feasible to use the numerical outcomes derived from the steady-state temperature field to assess the operational performance of BPHE during extended periods. Moreover, these outcomes facilitate the examination of whether the length of the heat exchanger is adequate and allow for the proposition of recommended lengths for the piping.

*4.1 Temperature Response and Its Steady-State Solution Under the Action of Heat Flux in Trigonometric Forms*

The analysis presented in Section 3.4 demonstrates that arbitrary heat flows exerted on BPHE can be decomposed into a step heat flux (direct current components) and a summation of heat fluxes represented as trigonometric functions using Fourier transform. While the effects of step heat flows have been discussed previously, the following analysis focuses on the impact of sinusoidal thermal flows on the temperature response.

*4.2 Temperature Response Under the Action of Heat Flux in Trigonometric Forms*

Heat flow expressed as a trigonometric function, termed as heat flux in trigonometric forms, possesses attributes consistent with trigonometric functions. Assuming the amplitude of such heat flow is defined as sin(2*pi*i/8760), and referencing parameters from Table 2, the temperature response at the borehole wall under this heat flux exhibits an initial rapid increase, followed by stabilization. The dimensionless excess temperature is invariant to the effects of the heat flow, and its variation trend is illustrated in Figure 9.

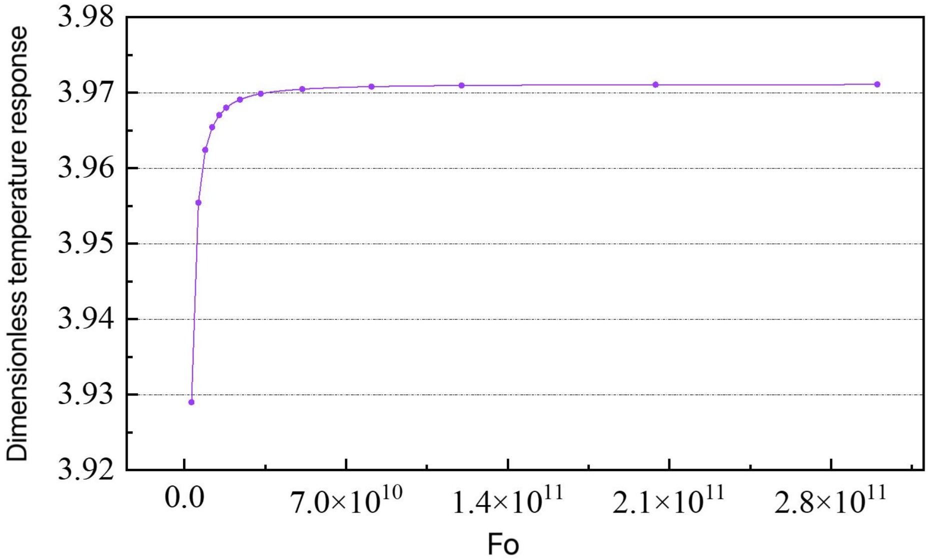


**Figure 9. Dimensionless Temperature Response at the Borehole wall under the Influence of the Heat Flux in Trigonometric Forms**

4.2.2 Steady-State Solution and Its Analysis of Temperature Response Induced by Heat Flux in Trigonometric Forms

Using MATLAB programming, the actual temperature response at the borehole wall was computed. Under the influence of trigonometric-form heat flux, the temperature response stabilizes at a consistent value after a sufficient period. This stable value corresponds to the steady-state solution, analogous to that induced by step heat flow. The resultant trend of this response is depicted in Figure 10.

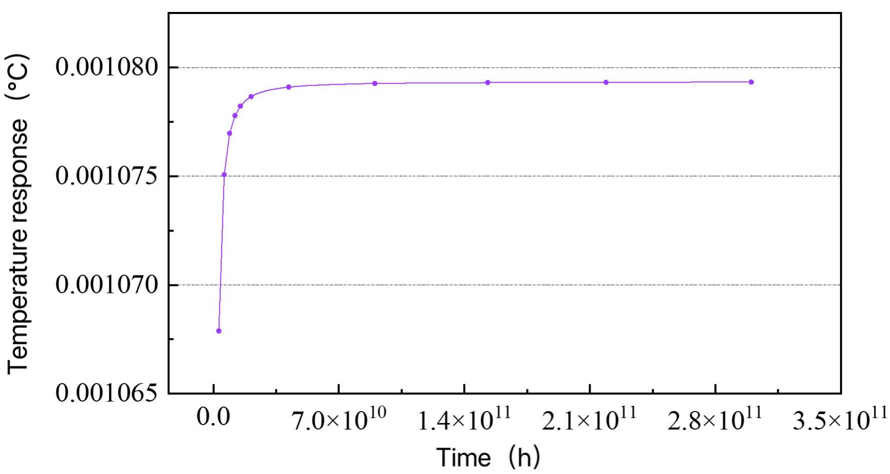


**Figure 10. Temperature Response at the Borehole wall under the Influence of Heat Flux in Trigonometric Forms Flow**

Figure 10 further demonstrates that, under the action of heat flux in Trigonometric Forms, the temperature response stabilizes at a consistent value after a sufficiently long period. This consistent value equates to the steady-state solution associated with the temperature response prompted by a step heat flow. Through the application of MATLAB programming and by calculating the limit as time approaches infinity, the steady-state solution of the temperature response for a heat flow $q_1$ is discerned to be 0.001079. Likewise, modifications to the heat flow $q_1$ parameters—namely amplitude, period, and phase angle—yield respective steady-state solutions of the temperature response as outlined in the subsequent table.

**Table 4. Steady-State Solutions of Temperature Response Under Thermal Flows with Various Amplitudes**

| Amplitude (W/m) | 1 | 10 | 20 | 30 | 40 |
|---|---|---|---|---|---|
| Steady-State Solutions of Temperature Response (℃) | 0.001079 | 0.010793 | 0.021586 | 0.032379 | 0.043173 |

Table 4 demonstrates the relationship between the amplitude of the heat flux and the steady-state solution of the temperature response. A larger amplitude corresponded to a higher steady-state temperature response, as depicted in Figure 7, indicating that the thermal load's intensity directly influences the equilibrium state of the BPHE.

**Table 5. Steady-State Solutions of Temperature Response Under Thermal Flows with Various Periods**

| Period (h) | 8760 | 4380 | 720 | 168 | 24 |
|---|---|---|---|---|---|
| Steady-State Solutions of Temperature Response (℃) | 0.001079 | 0.002158 | 0.013115 | 0.054976 | 0.075240 |

As shown in Table 5, the period of the heat flux significantly impacts the steady-state solution. However, for longer periods, the numerical value of the temperature response becomes negligible, reflecting the diminishing effect of low-frequency oscillations on the thermal equilibrium.

**Table 6. Steady-State Solutions of Temperature Response Under Thermal Flows with Various Phase Angles**

| phase angle (rad) | 0 | $\pi / 4$ | $\pi / 2$ | $3\pi / 4$ |
|---|---|---|---|---|
| Steady-State Solutions of Temperature Response (℃) | 0.001079 | 0.010716 | 0.015047 | 0.010563 |
| phase angle (rad) | $\pi$ | $5\pi / 4$ | $3\pi / 2$ | $2\pi$ |
| Steady-State Solutions of | -0.001079 | -0.010716 | -0.010716 | 0.001079 |

| Temperature Response (℃) |
|---|

The effect of the phase angle on the steady-state temperature response is presented in Table 6. While periodic variations in the phase angle induce cyclical changes in the steady-state response, the magnitude of these changes remains minimal, underscoring the relative stability of the BPHE under such conditions.

The aforementioned analysis elucidates that step heat flux precipitate variations in the temperature response of the soil surrounding the BPHE; conversely, the heat flux in trigonometric forms impart negligible effects on said temperature response. Consequently, in studying the temperature response of the soil surrounding the BPHE, it is possible to focus solely on the impact of step heat flow on the temperature response and disregard the influence of the heat flux in trigonometric forms to simplify the calculation procedures.

*4.3 Calculation Results*

By utilizing MATLAB programming, the heat flow acting on BPHE over a yearly cycle (period T=8760h, data point N=8760) are decomposed into a step heat flow (DC component) and the summation of (N/2-1) heat flux in trigonometric forms, using the method of Fourier transform.

The computational outcomes are tabulated in Table 7, detailing the calculated results for each parameter—comprising amplitude, period, and initial phase—for the leading 50 triangular waves with the maximal amplitudes. Concurrently, the system's direct current components, denoted as $a_0$ , amounts to 6.5514, which signifies the system's mean yearly heat flow measuring 6.5514W. Figure 11 presents the amplitude-frequency characteristics of the system, also referred to as the spectrum graphics. This representation offers the correspondence between sine wave amplitudes across varying frequencies following Fourier decomposition. It is evident from the analysis of the heat flow's amplitude-frequency characteristics that lower frequencies (longer periods) are generally associated with higher amplitudes, whereas higher frequencies (shorter periods) correspond to lower amplitudes. Additionally, it is observable that sine wave amplitudes across the vast majority of frequencies are minimal, suggesting a significant degree of stochastic variation in the heat flow exerted on the BPHE. Figure 12 depicts the phase-frequency characteristic graph of the heat flow, showcasing the correlation between sine waves and its initial phases at varying frequencies subsequent to Fourier transform. The graph indicates that initial phases oscillate within the range designated by $[-\pi, \pi]$ , suggesting pronounced stochasticity. This is largely due to the stochastic nature of the heat flux per unit borehole depth on the BPHE.

**Table 7. List of Parameters for the Top 50 Series with Maximum Amplitude**

| Amplitude | Period | Initial phase | Amplitude | Period | Initial phase |
|---|---|---|---|---|---|
| 21.99682 | 8760 | 2.76927 | 1.21204 | 350.4 | 1.24449 |
| 6.70173 | 24 | 2.48565 | 1.20296 | 199.0909 | 0.69372 |

| | | | | | |
|---|---|---|---|---|---|
| 3.88078 | 4380 | -0.74857 | 1.19561 | 8 | -0.2314 |
| 3.86512 | 2920 | 2.18192 | 1.19555 | 265.4546 | 0.04371 |
| 2.61456 | 730 | 0.45085 | 1.19511 | 250.2857 | 1.79978 |
| 2.58699 | 1095 | -0.58456 | 1.17949 | 673.8462 | -2.28552 |
| 2.47893 | 23.93443 | -1.1627 | 1.17081 | 224.6154 | -3.04197 |
| 2.44837 | 24.06593 | -0.06309 | 1.12101 | 162.2222 | -2.74775 |
| 2.35558 | 302.069 | -1.60236 | 1.08602 | 398.1818 | 0.91932 |
| 2.33072 | 625.7143 | -0.63671 | 1.08512 | 156.4286 | 1.06064 |
| 2.26687 | 336.9231 | 2.73738 | 1.07005 | 461.0526 | -2.30458 |
| 2.21088 | 168.4615 | -1.11761 | 1.04883 | 876 | -2.1526 |
| 1.8369 | 380.8696 | 1.91798 | 1.043 | 171.7647 | 2.50895 |
| 1.7985 | 796.3636 | -3.00812 | 1.03468 | 312.8571 | 0.60208 |
| 1.57209 | 12 | -0.78692 | 1.033 | 257.6471 | -1.41458 |
| 1.52966 | 219 | -0.23103 | 1.01911 | 1251.429 | -0.9258 |
| 1.48481 | 243.3333 | -1.64639 | 1.01517 | 282.5807 | -2.62775 |
| 1.4342 | 486.6667 | -0.91274 | 0.96469 | 21.00719 | 1.3089 |
| 1.40874 | 292 | 1.13531 | 0.94717 | 109.5 | -1.41092 |
| 1.36123 | 584 | 1.02684 | 0.91103 | 438 | -3.08989 |
| 1.35106 | 973.3333 | 2.22832 | 0.90812 | 515.2941 | 2.65254 |
| 1.32367 | 324.4444 | -0.76279 | 0.8773 | 213.6585 | 2.8057 |
| 1.2983 | 24.13223 | -2.95448 | 0.87609 | 547.5 | 2.18763 |
| 1.29432 | 23.86921 | 1.84087 | 0.86243 | 148.4746 | 2.22669 |
| 1.25605 | 6 | 2.85684 | 0.86193 | 120 | -1.65733 |

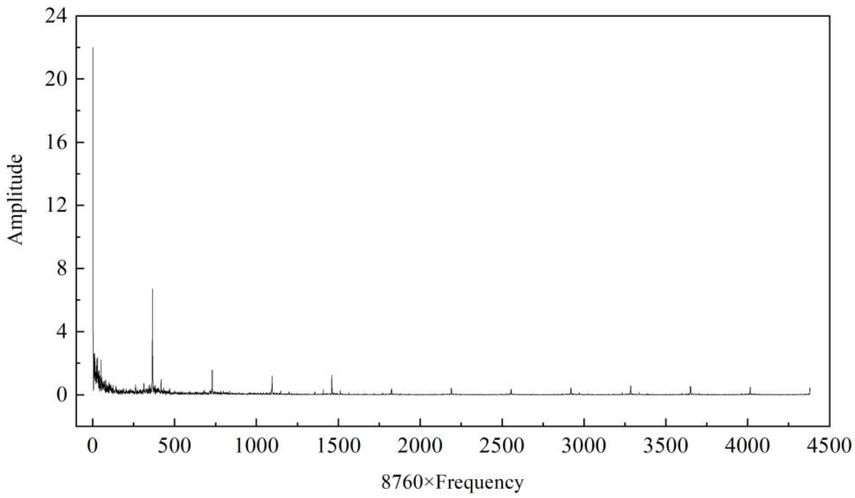


**Figure 11. Amplitude-Frequency Characteristic Graph of Heat Flow**

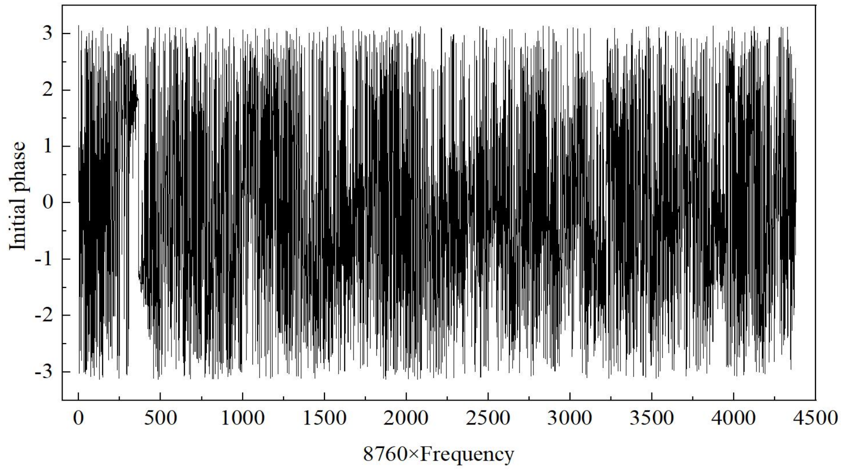


**Figure 12. Phase-Frequency Characteristic Graph of Heat Flow Discussion**

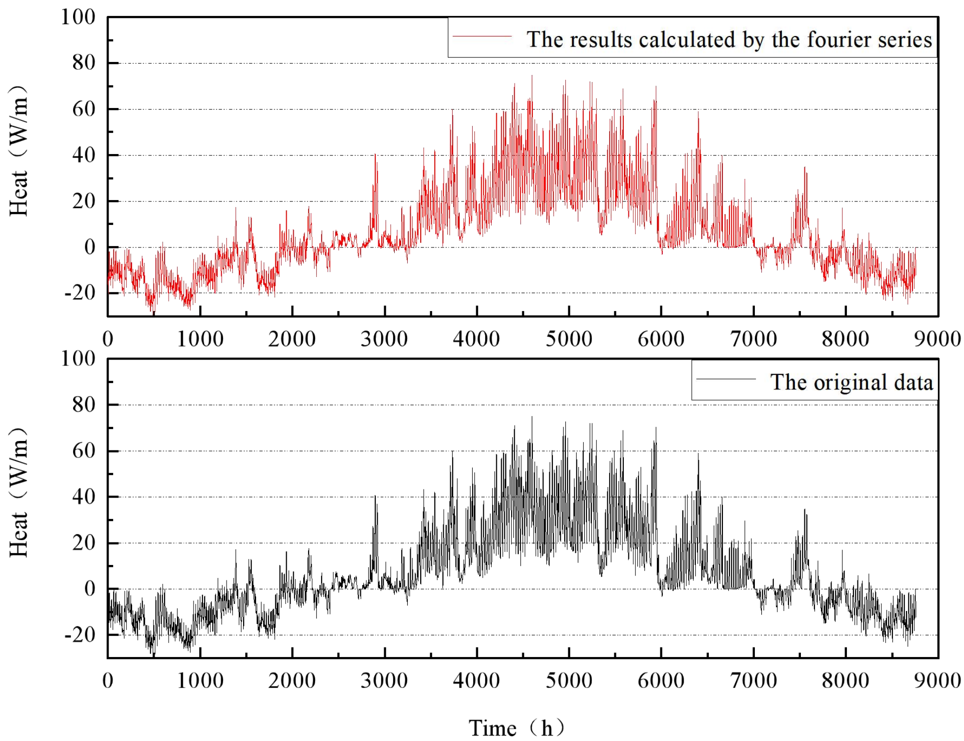


**Figure 13. Comparison Chart of the Results Calculated by the Fourier Series with the Original Data**

### *4.4 Error Analyses*

Utilizing the method previously described, the heat flux per unit borehole depth on the BPHE can be decomposed into a step heat flux (direct current components), and the summation of heat flux in trigonometric forms. To evaluate the computational precision of this algorithm, the results computed by the algorithm are compared with the original data, as depicted in Figure 13. Observation of Figure 13 reveals an almost complete congruence between the two datasets. Figure 14 displays the residuals of the data, demonstrating minimal absolute values of residual at each instance, all consistent at 0.13103 and demonstrating an alternating pattern of positive and negative fluctuations. The analysis of the results above indicates that the heat flow acting on the BPHE, when represented using a Fourier series, is of very high precision.

By employing the FFT, the heat flux per unit borehole depth exerted on the BPHE is decomposed with notable precision. The speed of computation is exceptionally expeditious, with the entire operation requiring a mere 3.4133 seconds.

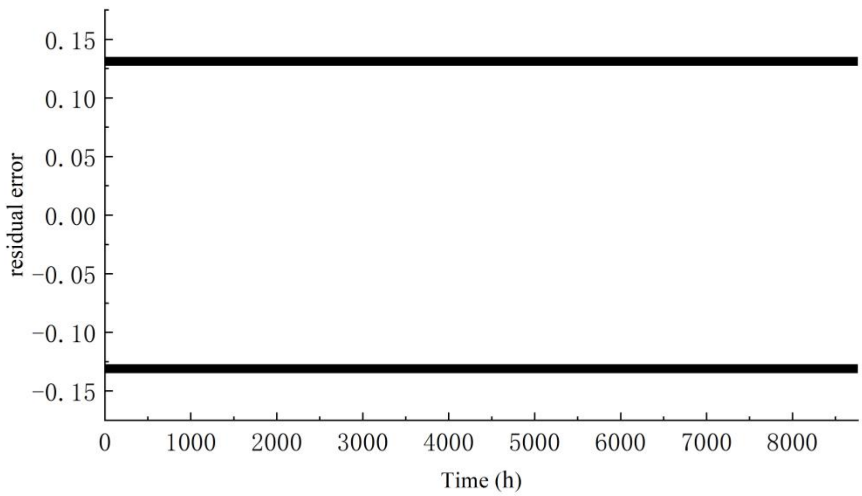


**Figure 14. Shows the Residuals between the Actual Values of the Heat Flow and the Sum of the Fourier Series**

## 5. Conclusion

The analysis within this study indicates that heat flows exerted on the BPHE can be decomposed into a step heat flux (direct current components), and the summation of heat flux in trigonometric forms. It is discerned that heat flux in trigonometric forms do not result in variations to the annual mean temperature of the soil surrounding the BPHE. In contrast, it is solely the step heat flow that prompts alterations in the annual mean temperature of the soil surrounding the BPHE. The conclusions were drawn as follows:

1. The long-term performance of the BPHE is exclusively governed by the step heat flow. The greater the step heat flow, the more significant the increase or decrease in the temperature of the rock and soil surrounding the GCHP after prolonged operation. This will severely affect the heat exchange performance of the BPHE, substantially weakening its heat exchange capacity to such an extent that it fails to meet the cooling and heating load requirements of the unit, causing the BPHE system to be unusable.

2. During the design phase of BPHE systems, it is imperative to minimize the annual periodic step heat flow to prolong the service life and ensure sustained high operational efficiency of the system.
3. In the case of systems demonstrating significant step heat flows following Fourier transformation, it is advisable to consider their utilization in conjunction with auxiliary systems, such as cooling towers and boiler systems. These supplementary systems could shoulder the entirety or a substantial portion of the step heat flow, thereby mitigating its impact.

**Acknowledgment**
This project is financially supported by the Department of Science and Technology of Henan Province, China (grant No. 242102240054).

**Reference**

Ahmadfard, M., & Bernier, M. (2019). A review of vertical ground heat exchanger sizing tools including an inter-model comparison Renew. *Sust. Energy. Rev*, 247-265. https://doi.org/10.1016/j.rser.2019.04.045

Cao, J., Zhou, S., Wang, T., Shan, B., & Liu, X. (2023). Research on a Variable Water Supply Temperature Strategy for a Ground-Source Heat Pump System Based on TRNSYS-GENOPT (TRNOPT) Optimization. *Sustainability*, *15*, 4388. https://doi.org/10.3390/su15054388

Cheruy, F., Dufresne, J. L., Aït Mesbah, S., Grandpeix, J. Y., & Wang, F. (2017). Role of soil thermal inertia in surface temperature and soil moisture-temperature feedback J. Adv. Model. *Earth Syst*, 2906-2919. https://doi.org/10.1002/2017MS001036

Choi, J.-S., Choi, S.-W., & Lee, E.-B. (2023). Modeling of Predictive Maintenance Systems for Laser-Welders in Continuous Galvanizing Lines Based on Machine Learning with Welder Control Data. *Sustainability*, *15*, 7676. https://doi.org/10.3390/su15097676

Cimmino, M. (2018). A finite line source simulation model for geothermal systems with series- and parallel-connected boreholes and independent fluid loops J. Build. Perform. *Simul*, 414-432. https://doi.org/10.1080/19401493.2017.1381993

Kitsopoulou, A., Zacharis, A., Ziozas, N., Bellos, E., Iliadis, P., Lampropoulos, I., Chatzigeorgiou, E., Angelakoglou, K., & Nikolopoulos, N. (2023). Dynamic Energy Analysis of Different Heat Pump Heating Systems Exploiting Renewable Energy Sources. *Sustainability*, *15*, 11054. https://doi.org/10.3390/su151411054

Kurevija, T., Macenić, M., & Galović, V. (2025). Regeneration of Rock Temperature Using Solar Thermal Energy Storage in Ground Source Heat Pump Systems-Sustainability for Regions with Both Heating and Cooling Needs. *Sustainability*, *17*, 1710. https://doi.org/10.3390/su17041710

Lamarche, L. (2017). Mixed arrangement of multiple input-output borehole systems Appl. *Therm. Eng*, 060. https://doi.org/10.1016/j.applthermaleng.2017.06.060

Lazzarotto, A. (2014). A network-based methodology for the simulation of borehole heat storage systems Renew. *Energy*, 265-275. https://doi.org/10.1016/j.renene.2013.07.020

Liang, M., Tu, J., Zeng, L., Zhang, Z., Cheng, N., & Luo, Y. (2023). Thermal Performance Analysis and Multi-Factor Optimization of Middle–Deep Coaxial Borehole Heat Exchanger System for Low-Carbon Building Heating. *Sustainability*, *15*, 15215. https://doi.org/10.3390/su152115215

Mariam, S. (2023). *Fourier transform and Fourier series, Editor(s): Jorge García, Encyclopedia of Electrical and Electronic Power Engineering, Elsevier*, 622-626. https://doi.org/10.1016/B978-0-12-821204-2.00093-3

Miglani, S., Orehounig, K., & Carmeliet, J. (2018). *A methodology to calculate long-term shallow geothermal energy potential for an urban neighborhood Energy Build*, 462-473. https://doi.org/10.1016/j.enbuild.2017.10.100

Mitchell, M. S., & Spitler, J. D. (2019). Characterization, testing, and optimization of load aggregation methods for ground heat exchanger response-factor models Sci. *Technol. Built Environ*, 1036-1051. https://doi.org/10.1080/23744731.2019.1648936

Moulinec, H., & Suquet, P. (1994). *A fast numerical method for computing the linear and nonlinear mechanical properties of composites C R Acad Sci, Paris II*, 1417-1423

Moulinec, H., & Suquet, P. (1995). A FFT-based numerical method for computing the mechanical properties of composites from images of their microstructures IUTAM symposium on microstructure-property interactions in composite materials, Springer Netherlands 1995, 235-246. https://doi.org/10.1007/978-94-011-0059-5_20

Narsilio, G. A., & Aye, L. (2018) Shallow geothermal energy: An emerging technology A. Sharma, A. Shukla, L. Aye (Eds.), *Low Carbon Energy Supply: Trends, Technology, Management, Springer Singapore, Singapore* (pp. 387-411). https://doi.org/10.1007/978-981-10-7326-7_18

Orian, L., Yahav, B., Gonen, G., Ronny, R., & Shahar, K. (2023). *FourierPIM: High-throughput in-memory Fast Fourier Transform and polynomial multiplication, Memories - Materials, Devices, Circuits and Systems*, *4*, 100034. https://doi.org/10.1016/j.memori.2023.100034

Qian, J., Wu, J., Yao, L., Mahmut, S., & Zhang, Q. (2021). Comprehensive performance evaluation of Wind-Solar-CCHP system based on emergy analysis and multi-objective decision method. *Energy*, *230*, 120779. https://doi.org/10.1016/j.energy.2021.120779

Rekeraho, A., Cotfas, D. T., Balan, T. C., Cotfas, P. A., Acheampong, R., & Tuyishime, E. (2025). Cybersecurity Threat Modeling for IoT-Integrated Smart Solar Energy Systems: Strengthening Resilience for Global Energy Sustainability. *Sustainability*, *17*, 2386. https://doi.org/10.3390/su17062386

Smith, A., & Taylor, J. (2023). Long-term performance analysis of ground source heat pumps in urban settings. *Geothermics*, *110*, 102567.

Wang, Y., Zhang, L., & Zhao, X. (2024). Deep learning for signal processing: A comprehensive survey. *IEEE Signal Processing Magazine*, *41*(1), 15-30. https://doi.org/10.1109/MSP.2024.3382166

Wu, X., Li, Y., & Zhang, H. (2025). A comprehensive review of the latest advancements in ground source heat pump systems for building heating and cooling applications. *Renewable and Sustainable Energy Reviews*, *165*, 112923.

Wu, Y., Hou, L., Su, T., & Ma, Y. (2024). Simulation Study on Performance of Solar-Powered Desiccant Wheel and Ground Source Heat Pump Air Conditioning in Qingdao. *Sustainability*, *16*, 3105. https://doi.org/10.3390/su16083105

Zhang, Q., & Wang, L. (2023). Efficient use of Fast Fourier Transform for high-speed data analysis in wireless communications. *IEEE Transactions on Signal Processing*, *71*(5),763-774.

Zhang, R., & Huang, Y. (2023). Advanced time-frequency analysis for non-stationary signals. *Elsevier Signal Processing*, *210*, 108123.

Zhou, Y., Narsilio, G. A., Soga, K., & Aye, L. (2024). Achieving Pareto Optimum for Hybrid Geothermal–Solar (PV)–Gas Heating Systems: Minimising Lifecycle Cost and Greenhouse Gas Emissions. *Sustainability*, *16*, 6595. https://doi.org/10.3390/su16156595

Diao, N. R., & Fang, Z. H. (2006). *Underground pipe ground source heat pump technology*. Beijing: Higher Education Press.